Supplement of Clim. Past, 19, 2053–2077, 2023
https://doi.org/10.5194/cp-19-2053-2023-supplement

Climate of the Past
Open Access
EGU

Supplement of

The hydrological cycle and ocean circulation of the Maritime Continent in the Pliocene: results from PlioMIP2

Xin Ren et al.

Correspondence to: Xin Ren (xinxin.ren@bristol.ac.uk)

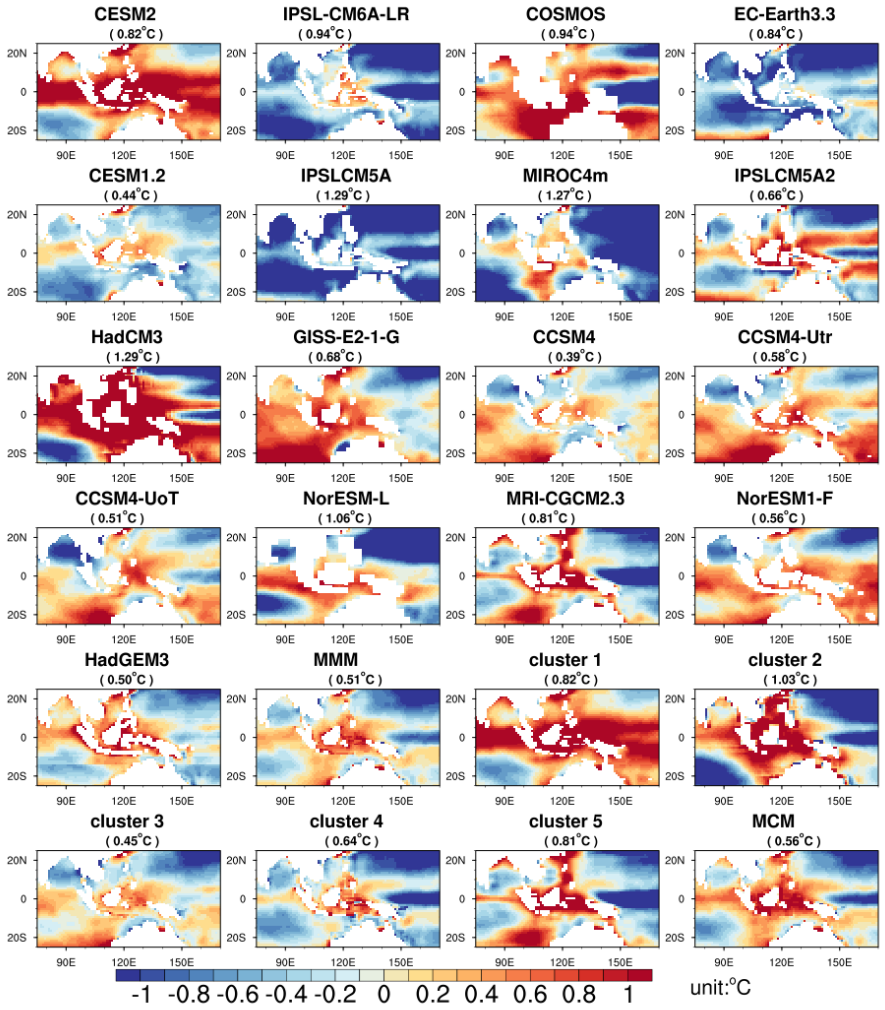

Figure S1. SST anomalies over the MC from individual models in the pre-industrial (E280) relative to HadISST1 reanalysed SSTs. Numbers in brackets indicate the RMSE between HadISST1 SSTs and model SSTs over the MC for each model.

Table S1. Discrepancy between individual model and data. Discrepency for Eoi400 is with respect to reconstruction, for E280 with respect to HadISST reanalysis. Unit:°C

Model name	Eoi400 discrepancy	E280 discrepancy	E280 discrepancy (bias adjusted)
CESM2	2.28	0.82	0.63
IPSL-CM6A-LR	1.58	0.94	0.56
COSMOS	1.73	0.94	0.91
EC-Earth3.3	2.17	0.84	0.53
CESM1.2	1.77	0.44	0.35
IPSLCM5A	1.52	1.29	0.62
MIROC4m	1.62	1.27	0.92
IPSLCM5A2	1.58	0.66	0.65
HadCM3	1.52	1.29	1.14
GISS-E2-1-G	1.52	0.68	0.64
CCSM4	1.58	0.39	0.39
CCSM4-Utr	1.93	0.58	0.52
CCSM4-UoT	1.62	0.51	0.50
NorESM-L	1.62	1.06	0.96
MRI-CGCM2.3	1.58	0.81	0.81
NorESM1-F	1.62	0.56	0.54
HadGEM3	2.08	0.50	0.50
MMM	1.58	0.51	0.50
cluster 1	2.28	0.82	0.63
cluster 2	2.28	1.03	1.03
cluster 3	1.58	0.45	0.44
cluster 4	1.58	0.64	0.55
cluster 5	1.58	0.81	0.81
MCM	1.62	0.56	0.56

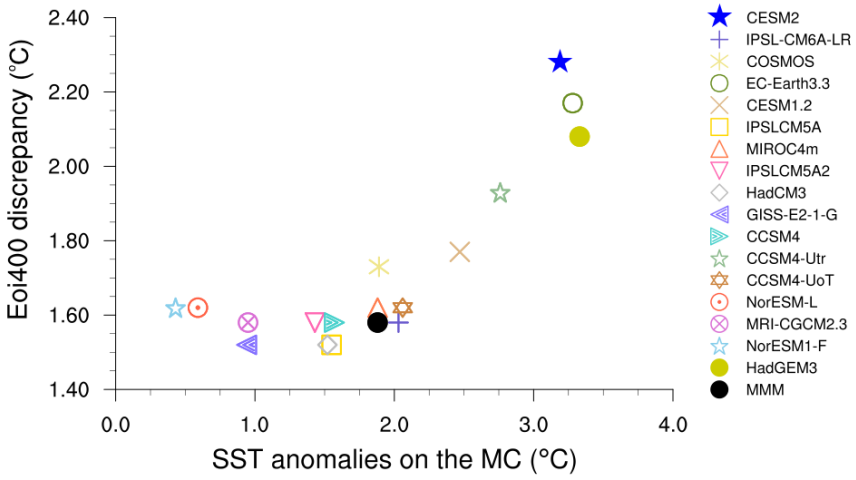

Figure S2. Comparison of the SSTAs averaged over the MC to the Eoi400 discrepancy with proxy. Discrepancy values are as shown in Table S1.

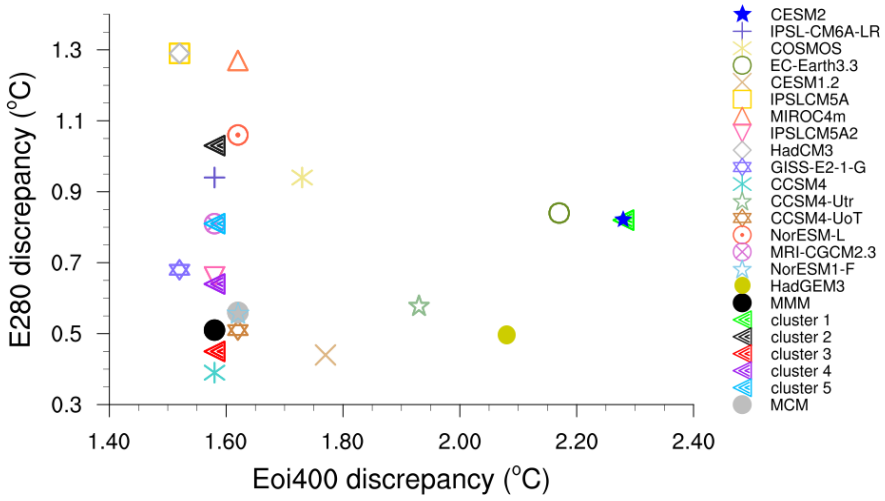

Figure S3. Comparison of the model-data discrepancies of the MC between the E280 and Eoi400 simulations. Discrepancy values are as shown in Table S1. The uncertainty of the Eoi400 discrepancies can be seen in Fig.3b of the manuscript. The unit is °C.

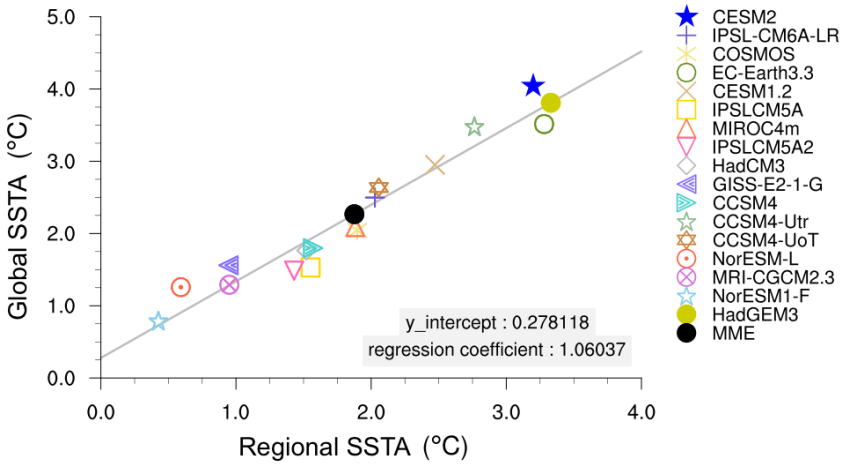

Figure S4. Comparison of the global SSTAs and the mean SSTAs over the MC.

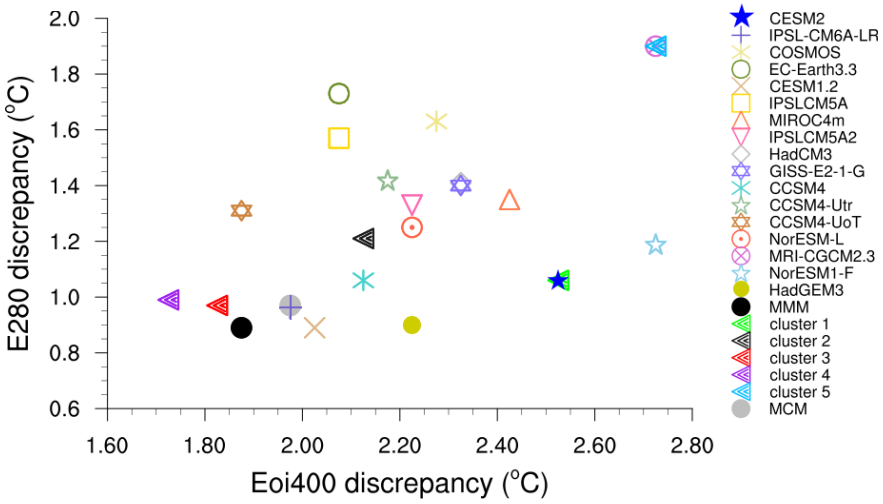

Figure S5. Comparison of model-data discrepancies at the global scale between the E280 and Eoi400 simulations.

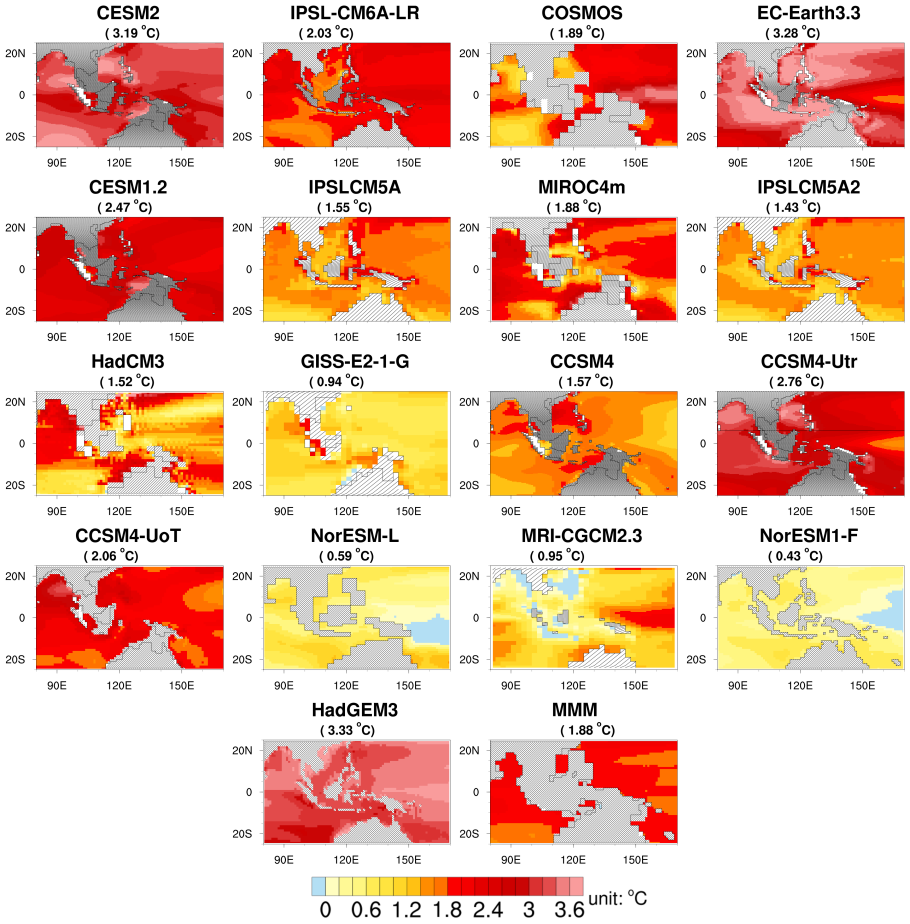

Figure S6. SSTA over the MC from individual models in the mid-Piacenzian warm period simulation (Eoi400) relative to the preindustrial simulation (E280). Numbers in brackets indicate the regional mean SST anomalies for each model.

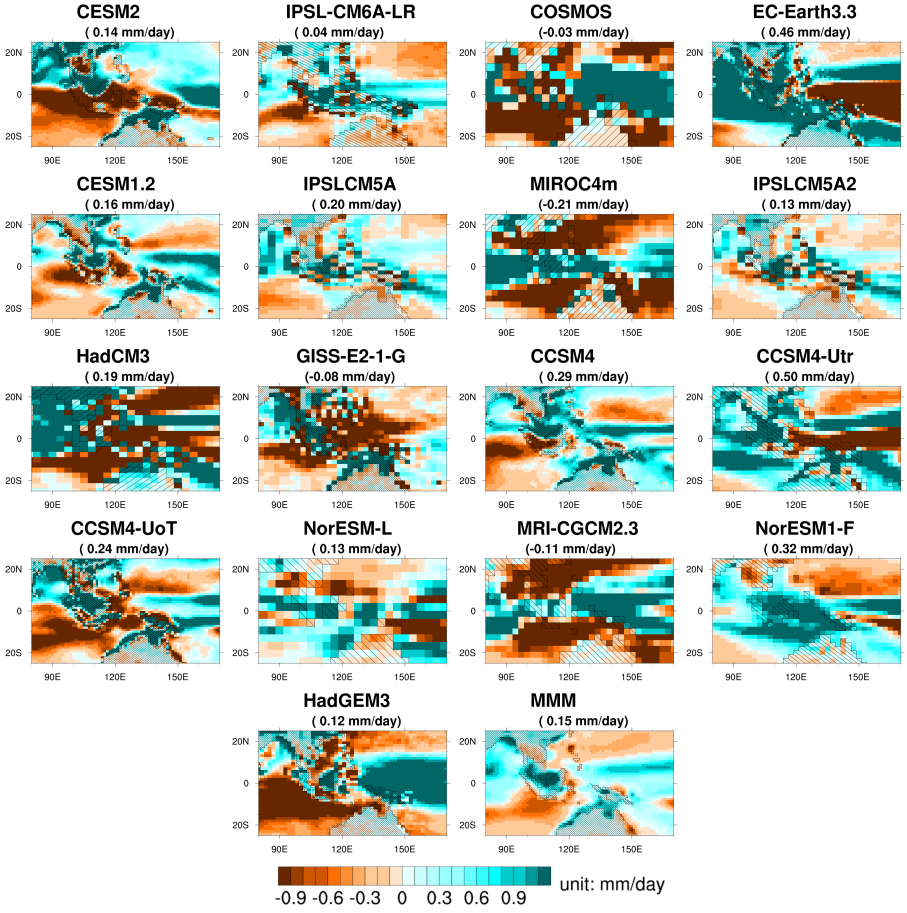

Figure S7. As Figure S6, but for precipitation minus evaporation (P-E).

Table S2. Proxy data in terms of wetter, drier or non-change condition used in Fig. 4b.

No.	Description	Proxy	Reference
0		paleolakes/diatomaceous sediment	Owen and Uthaaroon (1999)
1	weakened east asian monsoon; less Asian aridification	benthic and planktonic foraminiferal record; terrigenous sediment	Li et al. (2004); Wan et al. (2006)
2	less fertility of surface water, weakened East Asian winter monsoon	planktonic foraminifers δ13C	Jian et al. (2003)
3	In the late Pliocene, the climate gradually became drier, but it was substantially wetter than today.	palynofloras	Martin and McMinn (1994); Martin (2006)
4	In northeastern Australia, tropical warm conditions prevailed throughout the Pliocene.	based on the evolution of both plants and animals	Archer and M (1976); Travouillon et al. (2017)
5	Northwestern continent was more humid during the Pliocene period	potassium, thorium and uranium, as well as common clay minerals	Christensen et al. (2017)
6	Casuarinaceae–savanna has been reconstructed for the interior implying a warmer and wetter climate than today	fossil pollen- and spore-based estimates	Macphail (1997)
7	The sedimentary characteristics of the fluvial and lacustrine sediments suggests that this was an interval of intermittent stream flow under relatively arid conditions	lake deposition	(Alley, 1998; Macphail et al., 1994)
8	ever-green rain forest was still confined to the coastal mountainous areas, with rainfall levels similar to present	NAN	Macphail (1997); Martin Helene and Andrew (1993)
9	insignificant change	NAN	Macphail (1997); Martin Helene and Andrew (1993)
10	insignificant change	NAN	Kershaw and Sluiter (1982)

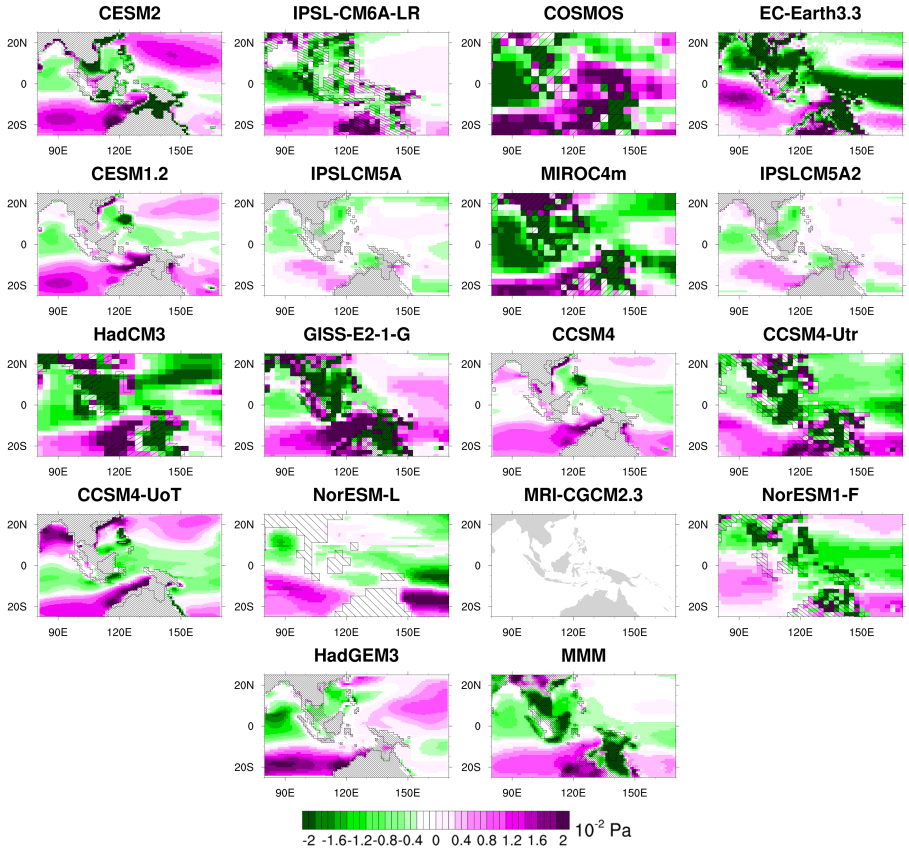

Figure S8. As Figure S6, but for zonal wind stress. Green shading indicates westward tendency, yellow shading indicates eastward tendency. Figure for MRI-CGCM2.3 is blank due to data availability. Unit: Pa.

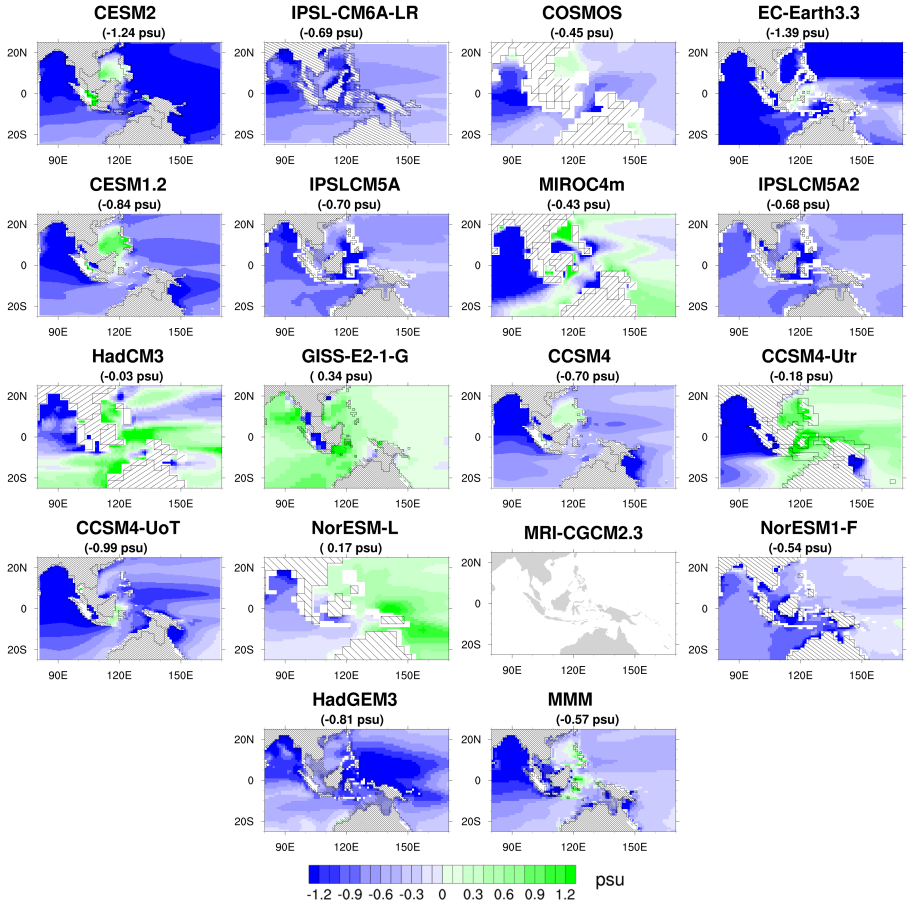

Figure S9. As Figure S6, but for sea surface salinity (SOS). Figure for MRI-CGCM2.3 is blank due to data availability.

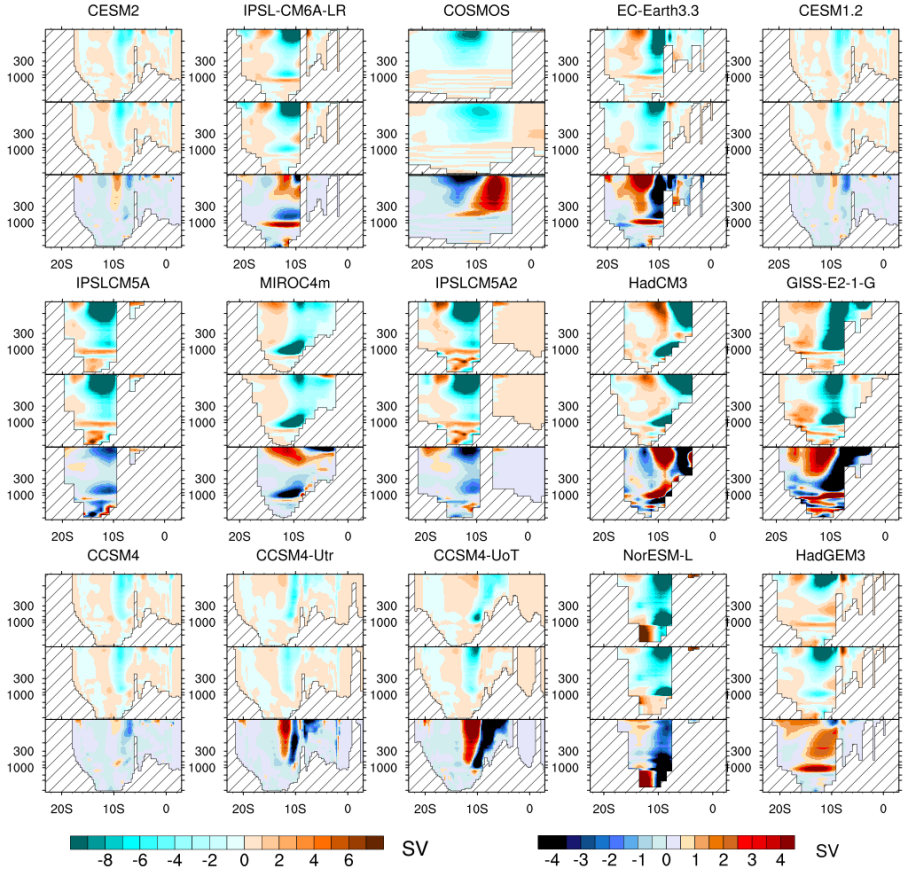

Figure S10. Profiles of the volume absolute transport of Timor strait in the mid-Piacenzian warm period (mPWP) (top panel for each model), in the preindustrial (middle panel for each model) and anomaly of the mPWP relative to preindustrial (bottom panel for each model). Warm shading indicates direction from west to east. Cold shading indicates direction from east to west. Left color bar for absolute transport (top and middle panel), right color bar for anomaly.

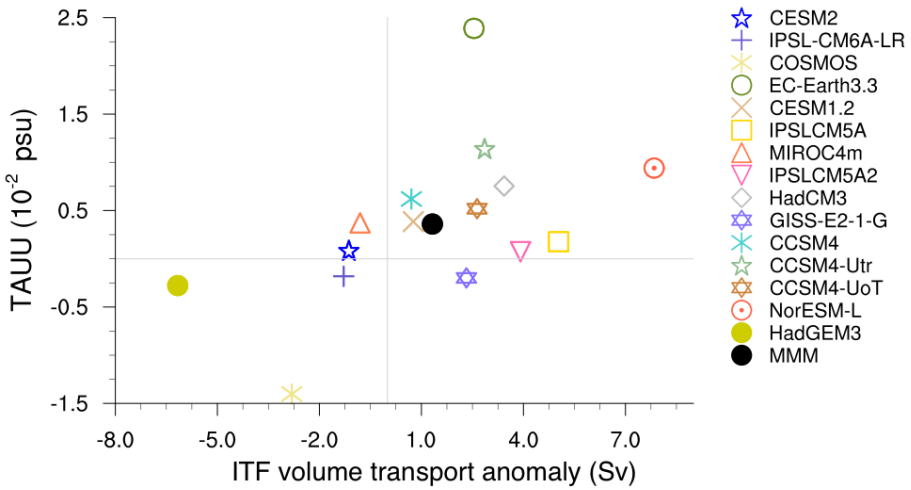

Figure S11. Comparison of the ITF volume transport anomalies and the western tropical Pacific (5S–5N, 120E–180E) zonal wind stress (TAUU) anomaly of the mid-Piacenzian warm period relative to preindustial.

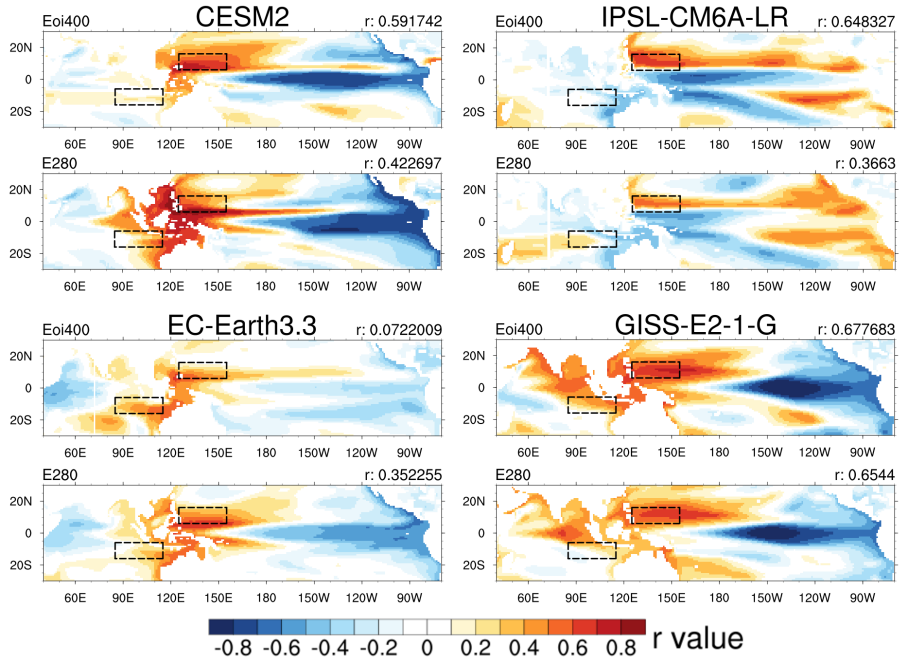

Figure S12. Map of linear regression coefficients in the annual SSH onto the annual ITF volume transport. Regions in black rectangles indicate western Pacific Ocean (6N – 16N, 125E – 155E) and eastern Indian Ocean (6S – 16S, 85E – 115E) regions for the calculation of the SSH gradient. The selection of the regions refers to Shilimkar et al. (2022). The r-value on the right top of each figure is the regression coefficient of the ITF volume transport and the SSH gradient between the western Pacific Ocean and the eastern Indian Ocean.

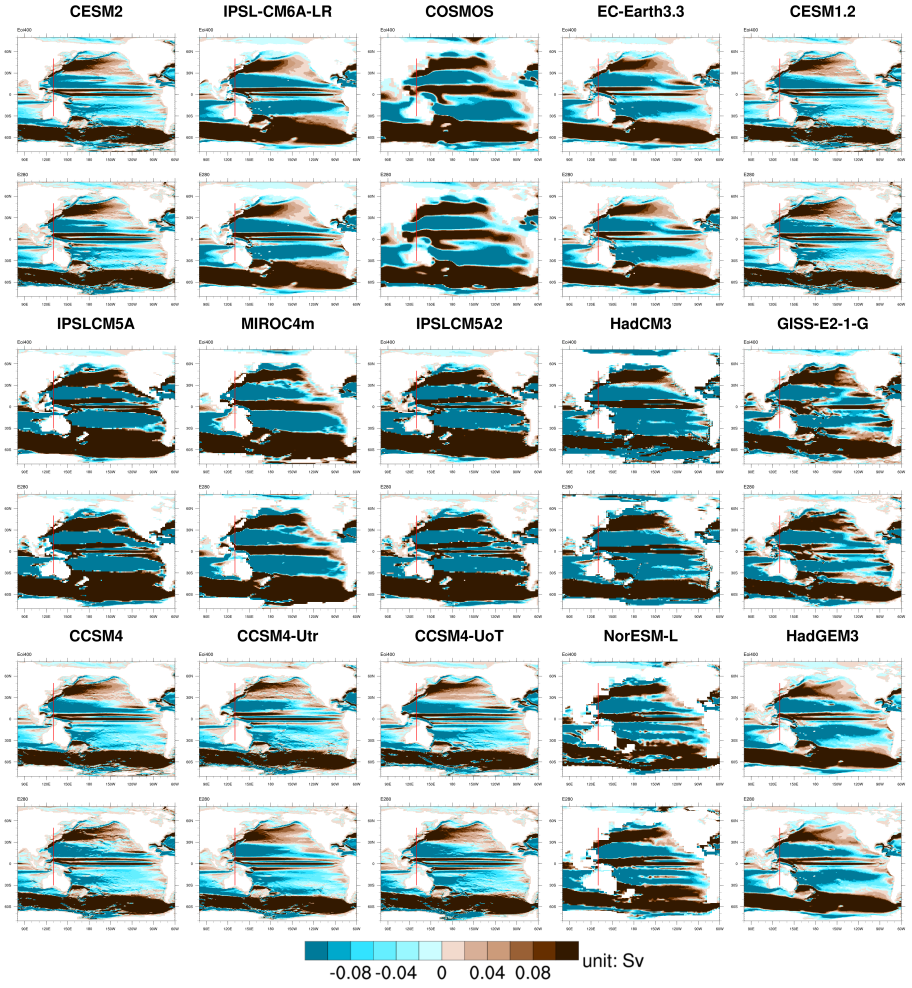

Figure S13. Zonal ocean volume transport intensity from individual models in the mid-Piacenzian warm period simulation (Eoi400) and the preindustrial simulation (E280). Red lines indicate transectes for the calculation of the total volume transport of the ITF.

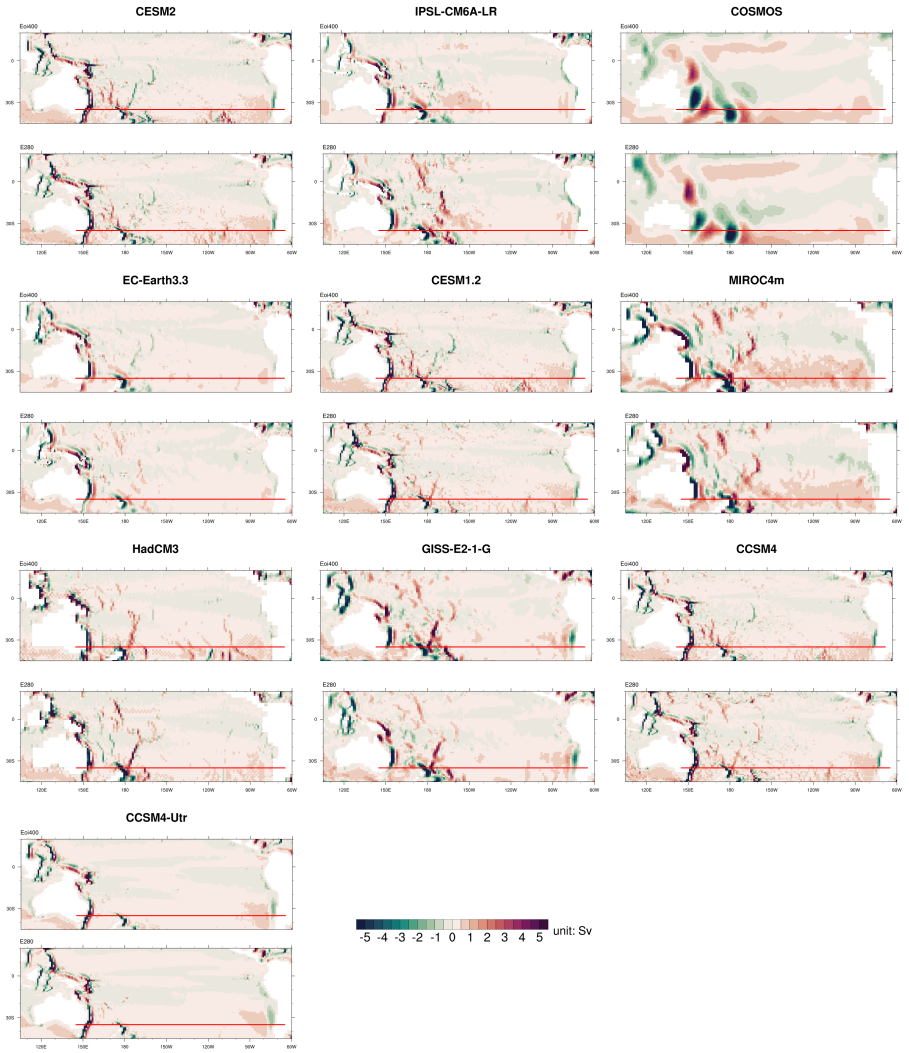

Figure S14. Meridional ocean volume transport intensity over the southern Pacific basin from individual models in the mid-Piacenzian warm period simulation (Eoi400) and the preindustrial simulation (E280). Red lines indicate transectes for the calculation of the volume transport into the Pacific basin. There are less models than Figure S13 due to data availability.

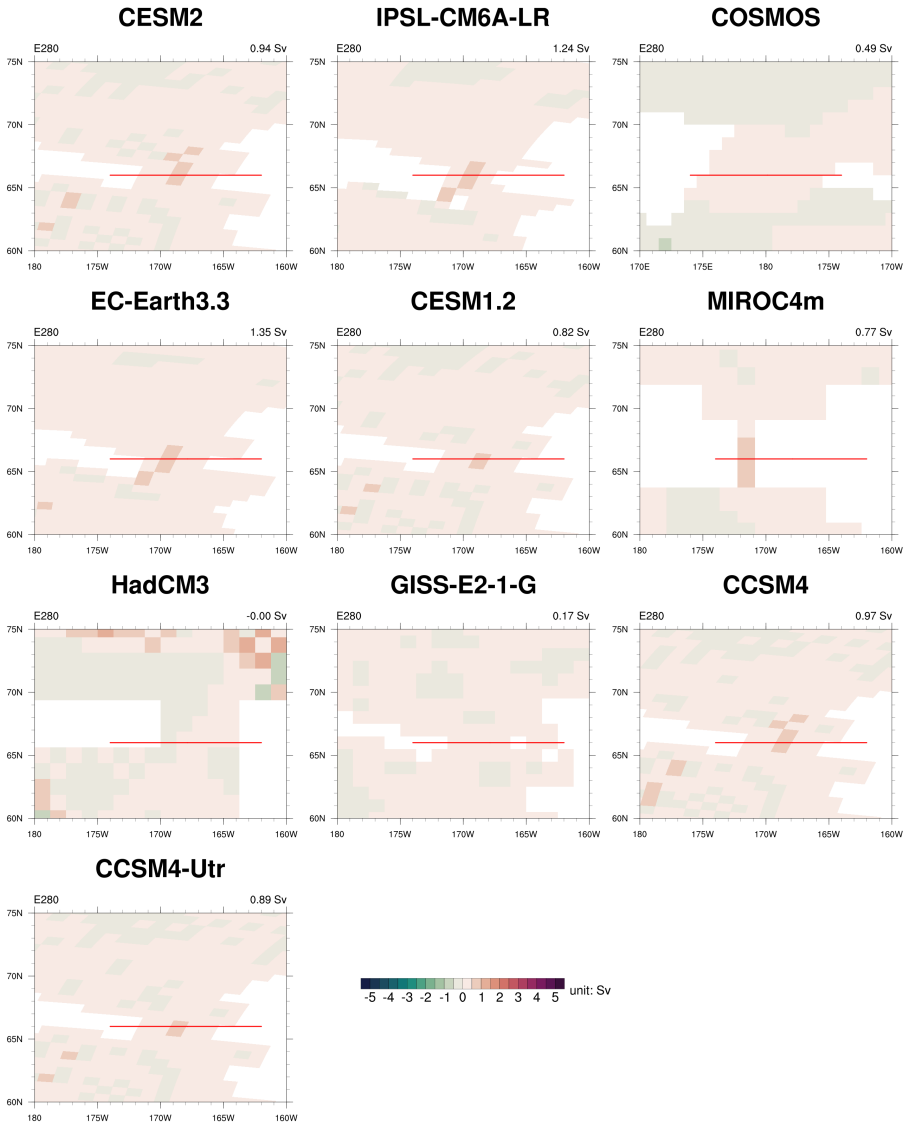

Figure S15. The meridional ocean volume transport intensity through the Bering Strait from individual models in the mid-Piacenzian warm period simulation (Eoi400) and the preindustrial simulation (E280). Red lines indicate transects for the total volume transport of the Bering Strait. There are less models than Figure S13 due to data availability.

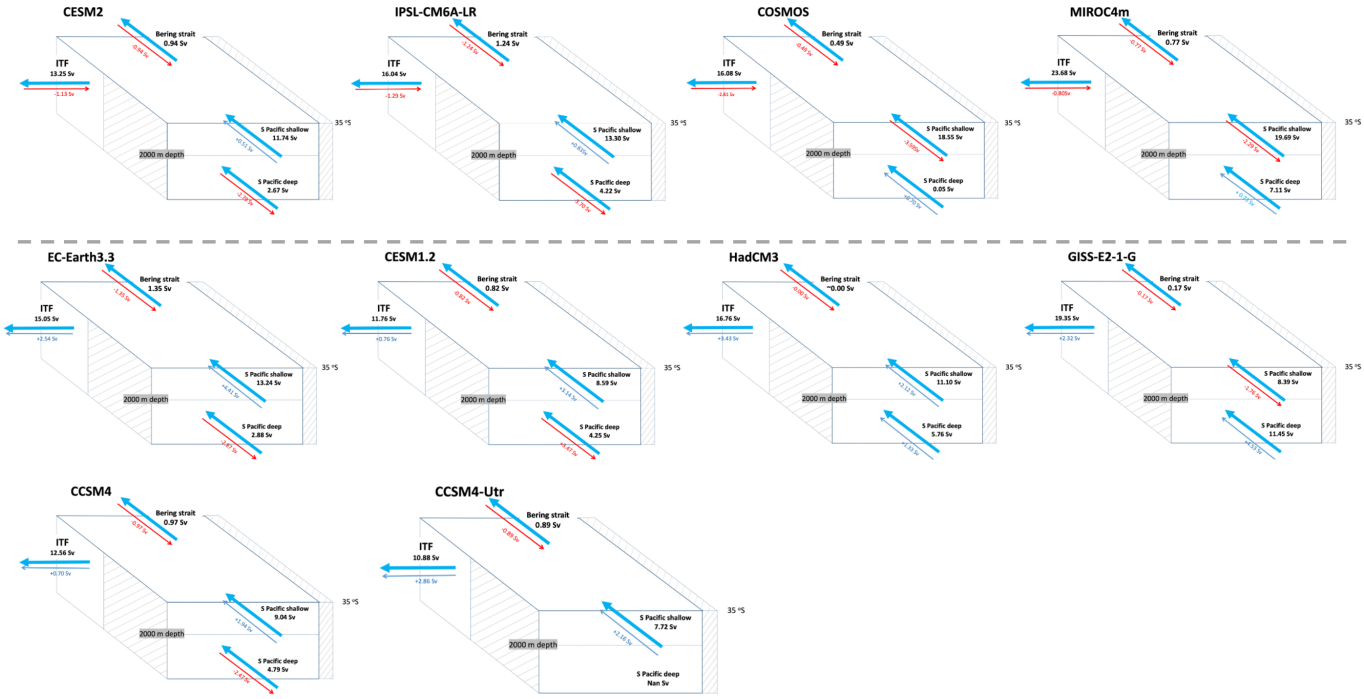

Figure S16. Schematic showing mean preindustrial flow direction (thick blue arrows) and the changes in the mid-Piacenzian warm period compared with the preindustrial (blue and red thin arrows) in the Pacific Basin (north of 35°S), Bering Strait and Indonesian Throughflow. The flow into the Pacific basin from the south is calculated from the shallow water above 2000 meters depth and deep water below 2000 meters depth. Blue and red for thin arrows indicate increased and decreased transport, respectively. Top panel (figures above grey dash line) shows models with decreased ITF volume transport; bottom panel (figures below grey dash line) shows models with increased ITF volume transport.